A User Material Subroutine for Progressive Failure Analysis of Woven Polymer-Based Composites Subjected to Dynamic Loading

David R. Hufner and Michael L. Accorsi

University of Connecticut, Storrs, CT, 06269

Abstract: *Woven polymer- based composites are currently used in a wide range of naval applications. Use of composite materials in critical applications requires that dynamic material behavior be fully characterized. Composite material behavior is generally well understood in the linear regime, and can be predicted with sufficient confidence up to the point of first ply failure. However, the mechanical behavior beyond first ply failure is not characterized by a validated theory that can account for material nonlinearity, strain rate dependence, and progressive failure. The objective of this work is to develop and validate a progressive failure approach that can be used for woven fabric polymer-based composites subjected to dynamic loads. The theory is implemented in Abaqus using a user material subroutine (UMAT) that defines the constitutive theory and implements the progressive failure methodology. Additionally, a deformation based failure criterion is developed, implemented, and validated against experimental observations. The progressive failure approach is validated using basic tension and open hole tension tests. The tests are performed using digital image correlation, which provides the complete non-uniform strain and displacement fields. Thus far, the comparison of simulation results to digitally imaged test data has been encouraging.*

Keywords: *Composites, Constitutive Model, Experimental Verification, Failure, Polymer*

1. Introduction

For many shipboard applications, composite materials are advantageous due to their high strength to weight ratio, ease of fabrication into curved geometries, and their acoustic and damping properties. The designs of many composite components are controlled by transient dynamic loadings. Compared to normal operating loads, these events are typically severe, and involve much higher loads and pressures. It is no surprise that linear analysis techniques, coupled with standard interactive failure criterion (e.g., Tsai-Wu, Tsai-Hill), predict lamina level (ply) failures for significant portions of the structure. Due to the uncertainty in predicting the nonlinear response of composites, the current design practice is to require that the composite remain linear (and undamaged) under even the most severe design loads. Attempting to design composite components using a linear response criterion often results in thicker, heavier, more expensive designs that do not take full advantage of the benefits of composites. Woven composites have high toughness, damage tolerance, and considerable durability. These materials can support considerably more load than that which initiates ply failure. The ability of composite materials to perform well after the onset of damage has been demonstrated experimentally, both statically and dynamically. However, because the mechanical behavior beyond first ply failure is not well characterized by a validated theory that can account for material nonlinearity, strain rate dependence, and progressive failure, the ability to demonstrate the adequacy of composite systems analytically is severely compromised.

In light of these limitations, the objective of this work is to develop and validate a progressive failure approach that can be used for woven fabric polymer based composites subjected to dynamic loads. The focus is on a select group of woven fabric E-Glass / Vinyl Ester composites that are commonly used on ship construction. The constitutive theory characterizes the mechanical behavior for fully non-linear anisotropic behavior under dynamic loading, and also accounts for strain rate dependence. Rate dependent failure criterion, in terms of deformation, is also proposed. The approach is validated using standard laboratory tests, as well as open-hole tension tests using digital image correlation technology. Tests have been conducted for various fiber orientations, and different strain rates.

A progressive failure theory is an analytical method in which a material's stiffness properties are incrementally degraded as failure occurs and progresses. A progressive failure theory consists of three main elements; 1) a constitutive law to describe the linear or non-linear stress versus strain behavior, 2) a failure theory to identify when a material point has reached failure, and 3) a degradation model to describe to the post-failure mechanical behavior. In the literature, there are *many* theories which address progressive failure (Soden, et. al., 2004). However, very few are capable of predicting nonlinear, large-strain, rate-dependent behavior to failure with a reasonable level of confidence. Moreover, few are linked to finite element codes to facilitate design application. In this work, a progressive failure approach is developed and integrated with Abaqus/Standard in the form a user material subroutine (UMAT). The subroutine was programmed by the author, and is intended for use with finite strain shell elements (S3, S4, S4R) in implicit dynamic analyses.

2. Theory and Implementation

2.1 Constitutive Theory

To develop a constitutive theory that is appropriate for a woven polymer based composite, we must first consider the basic nature of the response. Although behavior in the fiber directions can often be approximated as linear, the response for off-axis load orientations is highly complex and exhibits significant non-linearity and very high strain to failure. A sample plot showing the response of a 45° specimen is shown in Figure 1. For discussion, the response can be separated into four zones, in which a different type of behavior is observed in each. As loading begins, an initial elastic response is observed (zone 1). The behavior is mostly elastic up to approximately 0.5% strain. At this point, matrix cracking begins to occur (zone 2). As the load increases, the density of the matrix cracks keeps increasing, and the response becomes non-linear. At about 4% strain (zone 3), the density of matrix cracks reaches a saturation level, and very few new cracks are formed. The concept of crack saturation, also known as the 'characteristic damage state' (Reifsnider and Case, 2002), is a natural phenomena that occurs in many physical systems such as stratified rock or highway surfaces. Once a state of crack saturation is reached, the non-linearity resulting from matrix cracking is no longer prevalent. In this zone, the behavior is primarily controlled by the fibers. The fibers have a tendency to re-orient towards the direction of the loading vector. This behavior is referred to as trellising, and is said to occur whenever the angle between reinforcement directions changes from 90°. Fiber trellising continues until about 13% strain, where the fibers eventually begin to fail (zone 4). The final non-linearity is the likely result of statistically based fiber failure over a range of axial strain.

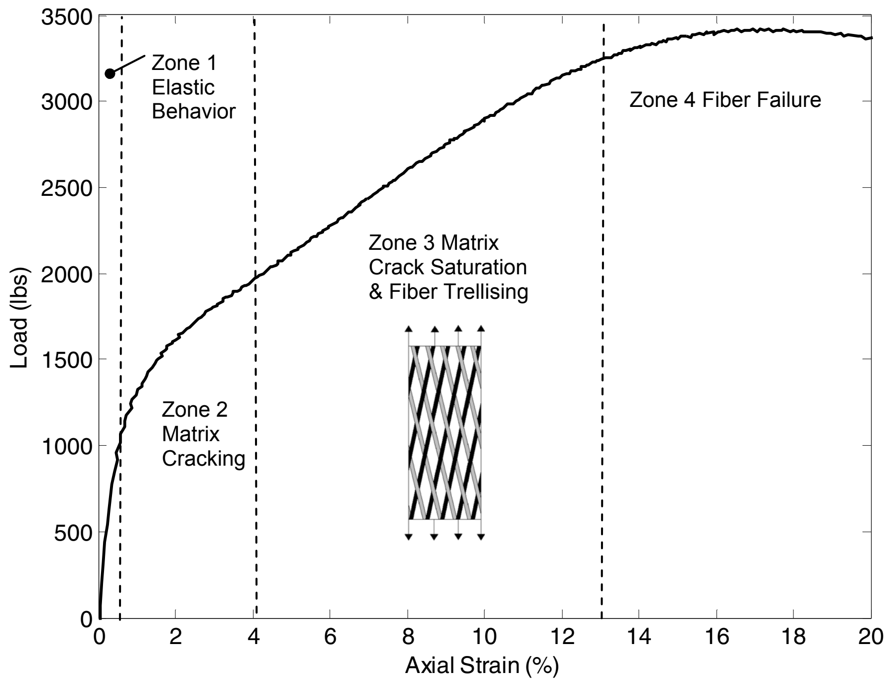

Figure 1. Typical off-axis response of woven composite.

The non-linear behavior for zones 1 and 2 occurs at relatively small strains and is suitable for characterization with continuum plasticity theory. Similar to classical plasticity theory in metals, it is convenient to work with 'effective' stress and strain values. The effective stress/strain in the composite is described using component values in material reinforcement directions. The convenience of this approach lies in the fact that non-linearity can be defined solely in terms of effective quantities. This implies that a potential function must exist, which characterizes the nonlinear aspects of the response. Sun & Chen (Sun and Chen, 1989) originally proposed a one parameter plastic potential function intended for unidirectional fibrous composites. Using the one parameter plastic potential function, Sun and Chen were able to describe a universal curve relating the effective stress ($\bar{\sigma}$) to the effective plastic strain ($\bar{\varepsilon}^{p}$). The one unknown parameter could be determined through a series of tension tests at various fiber reinforcement angles. If the effective stress vs. effective plastic strain curves for all test angles were plotted together, the correct value of the plasticity parameter would result in all curves collapsing to a single "master" curve. Sun and Chen were then able to fit the master curve with a power law equation of the form:

$$\bar{\varepsilon}^{p} = A\bar{\sigma}^{n} \tag{1}$$

where the constants A and n were determined from the curve fitting. Incorporation of non-linearity into an incremental plasticity analysis could then accomplished by obtaining a generalized plastic modulus, H_p, from differentiation of the assumed master curve fit.

$$H_{p} = \frac{d\bar{\sigma}}{d\bar{\varepsilon}^{p}} = \frac{1}{nA\bar{\sigma}^{n-1}} \tag{2}$$

For matrix dominated behavior, polymeric composites can exhibit noticeable rate-dependence. The rate dependence is incorporated into the theory by fitting the constant A to a second power law in terms of strain rate (Thiruppukuzhi and Sun, 2001).

$$A = \chi\left(\dot{\bar{\varepsilon}}^{p}\right)^{m} \tag{3}$$

Wherein, the constants χ and m are determined by curve fitting data from off axis tension tests at different strain rates. The exponent n in Equation 1 has been found rate *independent* (Weeks and Sun, 1997). Therefore, the rate dependence of the master curve is conveniently expressed in terms of a single rate dependent constant, A. The plastic modulus, H_p, can now be expressed in a strain rate dependent form by substituting Equation 3 into Equation 2.

$$H_{p} = \frac{1}{n\chi\left(\dot{\bar{\varepsilon}}^{p}\right)^{m}\bar{\sigma}^{n-1}} \tag{4}$$

The work of Sun and Chen was later expanded upon by Ogihara and Reifsnider (Ogihara and Reifsnider, 2002), who characterized non-linear behavior in woven glass/epoxy composites. Ogihara and Reifsnider observed that some plasticity did occur in fiber directions, and henceforth removed the assumption of linear behavior (i.e., vanishing plastic strain) in the fiber directions. This yielded a more general plastic potential, which consisted of four unknown parameters.

$$2f(\sigma_{ij}) = a_{11}\sigma_{11}^{2} + a_{22}\sigma_{22}^{2} + 2a_{12}\sigma_{11}\sigma_{22} + 2a_{66}\sigma_{12}^{2} \tag{5}$$

The constitutive theory used herein is derived from Ogihara and Reifsnider's plastic potential function. The reader is encouraged to consult this reference for the experimental procedure to determine the unknown parameters in Equation 5.

Incorporation of the constitutive theory into the user subroutine (UMAT) requires that a rate dependent material Jacobian matrix (tangent stiffness) be specified. The Jacobian is obtained through derivation of the material compliance matrix, C. The rate form constitutive law, written in terms of compliance, is:

$$\{\dot{\varepsilon}\} = [C]\{\dot{\sigma}\} \tag{6}$$

It is assumed that the strain rate, $\dot{\varepsilon}$, can be decomposed into the elastic and plastic rate components. Likewise, the compliance can be written as the sum of the elastic and plastic components.

$$\{\dot{\varepsilon}\} = \{\dot{\varepsilon}^e + \dot{\varepsilon}^p\} = (C^e + C^p) \cdot \{\dot{\sigma}\} \tag{7}$$

The elastic compliance, C^e in Equation 7, is expressed in terms of rate dependent elastic constants and the Poisson ratio ν_{12}.

$$C^e = \begin{bmatrix} \frac{1}{E_1^r} & -\frac{\nu_{12}}{E_1^r} & 0 \\ -\frac{\nu_{12}}{E_1^r} & \frac{1}{E_2^r} & 0 \\ 0 & 0 & \frac{1}{G_{12}^r} \end{bmatrix} \tag{8}$$

The rate dependent elastic constants are defined in terms of logarithmic functions, in which constants β and Γ are experimentally determined by testing at various strain rates. If no rate dependence is observed in the elastic behavior over a given range of strain rate, the rate dependence can optionally be suppressed by setting all $\beta = 0$ and all $\Gamma = 1$.

$$E_1^r = E_1(\beta_{11} \cdot \log \dot{\varepsilon}_{11} + \Gamma_{11}) \tag{9a}$$
$$E_2^r = E_2(\beta_{22} \cdot \log \dot{\varepsilon}_{22} + \Gamma_{22}) \tag{9b}$$
$$G_{12}^r = G_{12}(\beta_{12} \cdot \log \dot{\gamma}_{12} + \Gamma_{12}) \tag{9c}$$

Determination of the plastic portion of the compliance, C^p, is the primary focus of this discussion. We begin by calculating the plastic strain rate components from the potential function using an associated flow rule.

$$\dot{\varepsilon}_{ij}^p = \dot{\lambda} \cdot \frac{\partial f(\sigma_{ij})}{\partial \sigma_{ij}} \tag{10}$$

From Equation 5 and 10:

$$\dot{\varepsilon}_{11}^p = \dot{\lambda} \cdot (a_{11}\sigma_{11} + a_{12}\sigma_{22}) \qquad \dot{\varepsilon}_{22}^p = \dot{\lambda} \cdot (a_{22}\sigma_{22} + a_{12}\sigma_{11}) \qquad \dot{\varepsilon}_{12}^p = \dot{\lambda} \cdot (2a_{66}\sigma_{12}) \tag{11}$$

An equation for the proportionality factor rate ($\dot{\lambda}$) can be derived from the equivalence of the rate of plastic work, $\dot{W}^p$

$$\dot{W}^p = \overline{\sigma} \cdot \dot{\overline{\varepsilon}}^p = \sigma_{ij} \cdot \dot{\varepsilon}_{ij}^p \tag{12}$$

which states that the product of the effective stress and the effective plastic strain rate ($\dot{\bar{\varepsilon}}^p$) is the same as the tensor summation of the products of corresponding components. By substituting Equation 10 in Equation 12, and noting the definitions of effective stress and plastic modulus from plasticity theory, some manipulation yields an expression for the proportionality factor rate $\dot{\lambda}$.

$$\dot{\lambda} = \frac{9}{4 \cdot H_p \cdot \bar{\sigma}^2}\left[\left(a_{11}\sigma_{11} + a_{12}\sigma_{22}\right)\cdot \dot{\sigma}_{11} + \left(a_{22}\sigma_{22} + a_{12}\sigma_{11}\right)\cdot \dot{\sigma}_{22} + \left(2a_{66}\sigma_{12}\right)\cdot \dot{\sigma}_{12}\right] \tag{13}$$

Using Equation 13 in Equations 11, the plastic strain rate components are now available.

$$\begin{aligned}\dot{\varepsilon}_{11}^p = \frac{9}{4 \cdot H_p \cdot \bar{\sigma}^2}\Big[&\left(a_{11}^2\sigma_{11}^2 + 2a_{11}a_{12}\sigma_{11}\sigma_{22} + a_{12}^2\sigma_{22}^2\right)\cdot \dot{\sigma}_{11} \\ &+ \left(a_{11}a_{22}\sigma_{11}\sigma_{22} + a_{11}a_{12}\sigma_{11}^2 + a_{12}a_{22}\sigma_{22}^2 + a_{12}^2\sigma_{11}\sigma_{22}\right)\cdot \dot{\sigma}_{22} \\ &+ \left(2a_{11}a_{66}\sigma_{11}\sigma_{22} + 2a_{12}a_{66}\sigma_{12}\sigma_{22}\right)\cdot \dot{\sigma}_{12}\Big]\end{aligned} \tag{14a}$$

$$\begin{aligned}\dot{\varepsilon}_{22}^p = \frac{9}{4 \cdot H_p \cdot \bar{\sigma}^2}\Big[&\left(a_{11}a_{22}\sigma_{11}\sigma_{22} + a_{12}a_{22}\sigma_{22}^2 + a_{11}a_{12}\sigma_{11}^2 + a_{12}^2\sigma_{11}\sigma_{22}\right)\cdot \dot{\sigma}_{11} \\ &+ \left(a_{22}^2\sigma_{22}^2 + a_{12}a_{22}\sigma_{11}\sigma_{22} + a_{12}a_{22}\sigma_{22}^2 + a_{12}^2\sigma_{11}\sigma_{22}\right)\cdot \dot{\sigma}_{22} \\ &+ \left(2a_{22}a_{66}\sigma_{12}\sigma_{22} + 2a_{12}a_{66}\sigma_{11}\sigma_{12}\right)\cdot \dot{\sigma}_{12}\Big]\end{aligned} \tag{14b}$$

$$\begin{aligned}\dot{\varepsilon}_{12}^p = \frac{9}{4 \cdot H_p \cdot \bar{\sigma}^2}\Big[&\left(2a_{11}a_{66}\sigma_{11}\sigma_{12} + 2a_{12}a_{66}\sigma_{12}\sigma_{22}\right)\cdot \dot{\sigma}_{11} + \left(2a_{22}a_{66}\sigma_{12}\sigma_{22} + 2a_{12}a_{66}\sigma_{11}\sigma_{12}\right)\cdot \dot{\sigma}_{22} \\ &+ \left(4a_{66}\sigma_{12}^2\right)\cdot \dot{\sigma}_{12}\Big]\end{aligned} \tag{14c}$$

The terms preceding each of the stress rate components in Equations 14 correspond to components in the plastic compliance matrix, C^p. These matrix components are programmed into the user subroutine (UMAT). Since the combination of elastic and plastic compliance terms results in a fairly complex system of equations, a symbolic definition of the material Jacobian is not practical. Rather, The Jacobian is determined by forming the total compliance matrix and numerically inverting within the subroutine at each calculation point.

$$J = \left[C^e + C^p\right]^{-1} \tag{15}$$

To address the behavior is zone 3, the effective plastic strain at crack saturation is identified, and considered a material property in the analysis. Once the effective plastic strain reaches the specified value at crack saturation, the Jacobian matrix is held constant at its value when crack saturation is reached. Thereby, the constitutive theory is anisotropic linear in this zone. Analytically, the following condition is imposed.

$$\text{For} \qquad \bar{\varepsilon}^p > \bar{\varepsilon}^p_{sat} \;,\quad J = J_{sat} \tag{16}$$

2.2 Failure Theory

The choice of a failure theory should compliment the constitutive theory. In this case, a non-linear constitutive theory is used, in which the source of the non-linearity is sub-critical damage resulting from matrix cracking. Herein lies a significant benefit of the proposed theory; the damage mode attributable to matrix cracking is already accounted for within the constitutive theory and does not need to be addressed with mechanistic failure theories that predict matrix failure or the onset of matrix cracking. For this constitutive theory, the only lamina-level failure mechanism that must be addressed is fiber breakage. However, the large deformations experienced in off-axis loadings add a significant level of complication. The fibers are trellising and the reinforcement directions are no longer 90° apart. For a 45° specimen subjected to 20% strain, it is estimated that the reinforcement directions reach a point where they are only 70° apart. Therefore, the strains in the material coordinate system are no longer coincident with the fiber directions. In order for a failure theory to be successfully applied, the large deformation induced fiber trellising must be accounted for.

A mechanistic criterion that characterizes fiber failure at large deformations is proposed. This criterion is expressed entirely in terms of deformation, and is founded on two basic postulates. The first postulate is that lamina failure occurs when the strain in the rotated fiber direction reaches a critical value, which is independent of load orientation. Xing (Xing, 2007) has also recently suggested this concept. This leads to our second postulate, which is that the Green-Lagrange normal strain (in the material coordinate system) can act as a proxy for the strain in the rotated fiber. The Green-Lagrange normal strains are expressed in terms of the deformation gradient components in the material coordinate system. Thereby, failure functions can be constructed that are based entirely on deformation, and do not require the definition of load orientation. We adopt the general form of the failure function, similar to Reifsnider and Case (Reifsnider and Case, 2002):

$$Fa = Fa\left(\frac{e_{ij}}{\varepsilon_f}\right) \tag{17}$$

where the Green-Lagrange strain components in the numerator (e_{ij}) correspond to the direction and sense of the fiber failure strains (ε_f) in the denominator. In this case we use two failure functions (one for warp fibers and one for fill fibers), which imply fiber breakage when either of the Green-Lagrange normal strains (e_{11}, e_{22}) reaches the corresponding fiber failure strain. The Green-Lagrange finite strain tensor $[E]$ is calculated from the deformation gradient tensor $[F']$ as follows.

$$[E] = \frac{1}{2}\left([F']^T[F'] - [I]\right) \tag{18}$$

In this case, the deformation gradient tensor must be with respect to the material coordinate system. This is indicated by the prime superscript. Resulting Green-Lagrange strains will then be with respect to the material system. By using Equation 18, and substituting the Green-Lagrange normal strains into Equation 17, the failure functions can be expressed solely in terms of deformation gradient components.

$$Fa_{warp} = \left(\frac{(F'_{11})^2 + F'_{12}F'_{21} + F'_{13}F'_{31} - 1}{2\varepsilon_{f,warp}} \right) \qquad Fa_{fill} = \left(\frac{F'_{21}F'_{12} + (F'_{22})^2 + F'_{23}F'_{32} - 1}{2\varepsilon_{f,fill}} \right) \tag{19}$$

The fiber failure strains (ε_f) for warp/fill directions may be taken as the break strains observed in a 0° or 90° specimen tests. If necessary, these failure functions can include strain rate dependence by replacing the failure strains in warp/fill directions with the strain rate dependent functions:

$$\varepsilon_{f,warp} = \varepsilon^0_{f,warp}\left(\beta_f \cdot \log\dot{\varepsilon} + \Gamma_f\right) \qquad \varepsilon_{f,fill} = \varepsilon^0_{f,fill}\left(\beta_f \cdot \log\dot{\varepsilon} + \Gamma_f\right) \tag{20}$$

where ε_f^0 is the fiber failure strain for the reference strain rate, and β_f and Γ_f are material constants determined based on a logarithmic fit of failure strain vs. strain rate data. The failure functions become:

$$Fa_{warp} = \left(\frac{(F'_{11})^2 + F'_{12}F'_{21} + F'_{13}F'_{31} - 1}{2\varepsilon^0_{f,warp}\left(\beta_f \cdot \log\dot{\varepsilon} + \Gamma_f\right)} \right) \qquad Fa_{fill} = \left(\frac{F'_{21}F'_{12} + (F'_{22})^2 + F'_{23}F'_{32} - 1}{2\varepsilon^0_{f,fill}\left(\beta_f \cdot \log\dot{\varepsilon} + \Gamma_f\right)} \right) \tag{21}$$

It is likely that for low-intermediate strain rates there will be little, if any, rate dependence of the fiber failure strain. In such cases, the strain rate dependence can be suppressed by setting $\beta_f = 0$ and $\Gamma_f = 1$. In this regard, the proposed criterion has a significant advantage over traditional stress-based criterion. In stress criterion, failure strengths are often highly sensitive to strain rate. Failure strains have much lower rate sensitivity.

Since the deformation gradient components are already calculated by Abaqus, and are available from within the user subroutine, this failure criterion is quite suitable for implementation and use within the Abaqus framework.

2.3 Degradation Model

Degradation of the material point stiffness is begun once either failure function is greater than 1. Since the failure criterion already addresses final failure, the purpose of the degradation model is to maintain a level of computational stability, and provide a somewhat realistic characterization of the critical failure process. Due to the statistical nature of fiber failures, it is unlikely that constitutive matrix will instantaneously vanish. Degradation over a small range of increasing strain is more reasonable, and often provides for improved model convergence. Since degradation involves material softening, and softening is a strain controlled phenomena, it is a natural choice to define a degradation factor (ψ) in terms of the failure function value (above 1.0). The degradation factor is defined based on a decaying exponential form as follows.

$$\psi = \exp\left(-\frac{z^2}{2}\right) \qquad z = \frac{Fa - 1}{\mu} \tag{22}$$

where the variable z is calculated based on the failure function and a softening constant μ, which can be adjusted to control the amount of degradation for a given failure function. The Jacobian matrix (J) for the failed material point (Fa > 1) is then determined by multiplying the Jacobian matrix corresponding to the point where the failure function first equals 1 by the degradation factor ψ.

$$J^{Fa>1} = \psi J^{Fa=1} \tag{23}$$

However, the value of the Jacobian where the failure function first equals 1 is not accessible from within the subroutine. This issue is resolved by storing the degradation factor and the value of the Jacobian as state dependent variables (SDV) so their values from the previous step are available. If a material point is failed, the Jacobian for the current step is determined by correcting the previous value based on the previous value of ψ, and then multiplying the result by the current value of ψ.

$$J^{i} = \frac{\psi^{i}}{\psi^{i-1}} J^{i-1} \tag{24}$$

This procedure results in a degraded Jacobian matrix that is equivalent to Equation 23. To ensure that the Jacobian cannot increase between successive increments, which would imply "healing" behavior, the following condition is imposed on the degradation factor.

$$\psi^{i} \le \psi^{i-1} \quad \text{For} \quad Fa > 1 \tag{25}$$

3. Experimental

Experimental data is collected using digital image correlation. The tests were performed by Correlated Solutions Inc. (www.correlatedsolutions.com). Digital imaging is a non-contact measurement technique that uses no mechanical gauges and requires no mechanical interaction with the specimen. A servo-hydraulic test machine is used, while a high speed camera photographs the specimen at frequencies ranging from 10 to 2,000 Hertz. Using a proprietary software program, developed by Correlated Solutions, the displacements are determined by comparing positions of individual pixels in the image to their original positions in an undeformed reference image. Once the full displacement field is determined, the strain field is numerically calculated. The servo-hydraulic machine has an integrated load cell, and load measurements are synced to each photograph.

The benefits of this test method are the availability of the full strain/displacement field, as well as the ability to experimentally determine all components of strain (normal and shear) at any point in the area of interest. This is particularly useful in development of constitutive theory and failure theory. In these activities, the analyst often requires knowledge of all strain components (and their spatial variation), rather than just the strain in the loading direction at a single point. Another significant benefit of digital imaging is the ability to accurately measure low strains, as well as extremely large strains, within a single test. The low strain data often requires a high level of accuracy to perform modulus calculations, while the high strain data is needed to determine constitutive model parameters and characterize failure. If mechanical gauges are used, these data would require several tests with different gauges to collect.

Using digital imaging, basic tension and open hole tension specimens are tested at two different fiber angles (0° and 45°) and at different strain rates. The strain rates tested varied from low (0.0001 /s) to intermediate (0.1 /s) speed. The specimens were cut from a 10 ply E-glass / Vinyl ester panel, with a warps parallel lay-up and a plain weave pattern. Each ply was 0.016 inches thick, and the total thickness of the panel was approximately 0.16 inches. The rectangular test specimens were nominally cut 6 inches long and 0.8 inches wide. For the open hole specimens, the central hole was 0.2 inches in diameter. The gauge lengths had some variation between tests, but were generally in the range of 3.2 – 3.7 inches. Strain contour plots from digitally imaged open hole tension tests are shown in Figure 2 and Figure 3 for the 0° and 45° specimens. The corresponding load levels are equal to, or slightly less than, the failure load in each case. It is noted that strain contours for the 0° specimen transverse strain and 45° specimen shear strain appear highly discontinuous. In these instances, the strains are quite small and are close to the accuracy threshold of the measurement technique.

Additional testing was also performed at the University of Connecticut using a servo-hydraulic machine with a specially fabricated clip gauge to measure large deformation. The specimens tested at UConn were from the same panel as described above. The testing was performed using rectangular specimens that were approximately the same size as the digital image tests. Six different specimen angles where tested (0°, 15°, 30°, 45°, 60°, and 90°) at three different strain rates (0.0001 /s, 0.002 /s, 0.01 /s). These data were used to determine some of the constitutive model parameters associated with the master curve. A subset of these data was reported by Xing (Xing, 2007), and is also contained in a previous publication (Reifsnider and Xing, 2007).

Longitudinal Strain (ε_{yy}) Transverse Strain (ε_{xx}) Shear Strain (γ_{xy})

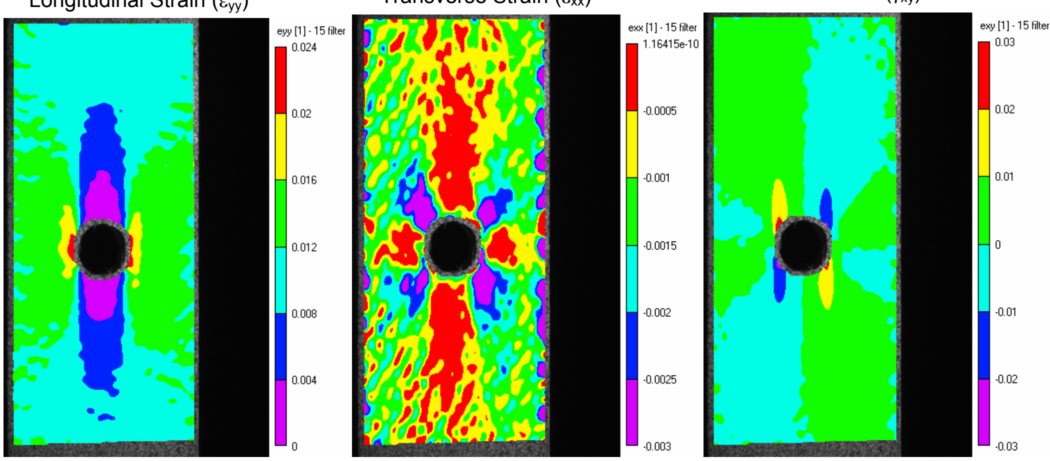

Figure 2. Open hole tension test, digitally imaged data for 0° specimen, 4447 lbs.

Longitudinal Strain (ε_{yy}) Transverse Strain (ε_{xx}) Shear Strain (γ_{xy})

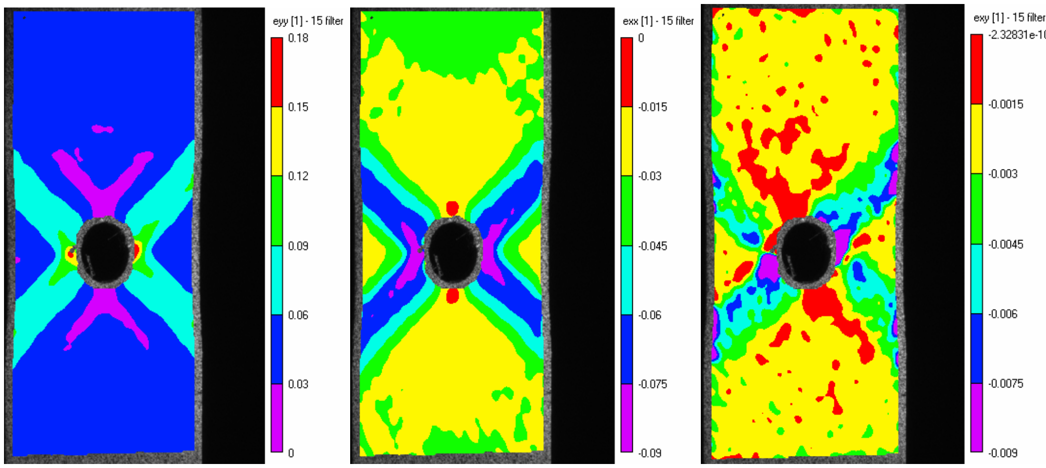

Figure 3. Open hole tension test, digitally imaged data for 45° specimen, 1948 lbs.

4. Simulation

Finite element simulations were performed in Abaqus/Standard and compared to the digital image test results. Dynamic simulations are performed for basic tension and open-hole tension 0° and 45° specimens. The progressive failure user input parameters are shown in Table 1.

Table 1. Model Input Parameters.

E_1 (psi)	E_2 (psi)	G_{12} (psi)	ν_{12}	a_{11}	a_{12}	a_{22}	a_{66}	n	m	$\bar{\varepsilon}^p_{sat}$	ε_f^0	μ
3.56E6	3.2E6	610,000	0.1	1	0.1	1.2	19.9	4.1	-0.16	0.006	0.023	0.05

A comparison of simulation results to test data is shown in Figure 4 for the 0° and 45° basic tension specimens. The simulation shows excellent agreement with experimental results. For the 0° and 45° open hole tension specimens, comparisons of simulation results to test data are shown in Figure 5 and Figure 6 respectively. Excellent agreement with experimental data is also observed for the open hole tension simulations. To generate the load vs. strain curves for the digitally image tests, an averaging procedure is used to account for the fact that the strain field is not perfectly symmetric about the hole. The data is for point 1 is obtained by averaging corresponding locations on the right and left sides of the hole. The data for point 3 is obtained by averaging corresponding locations at top dead center and bottom dead center locations. In similar fashion, the data for point 2 is obtained by averaging the four points that are in the same 45° relation to the hole. Points 1-3 are a radial distance of 0.2 inches from the hole center.

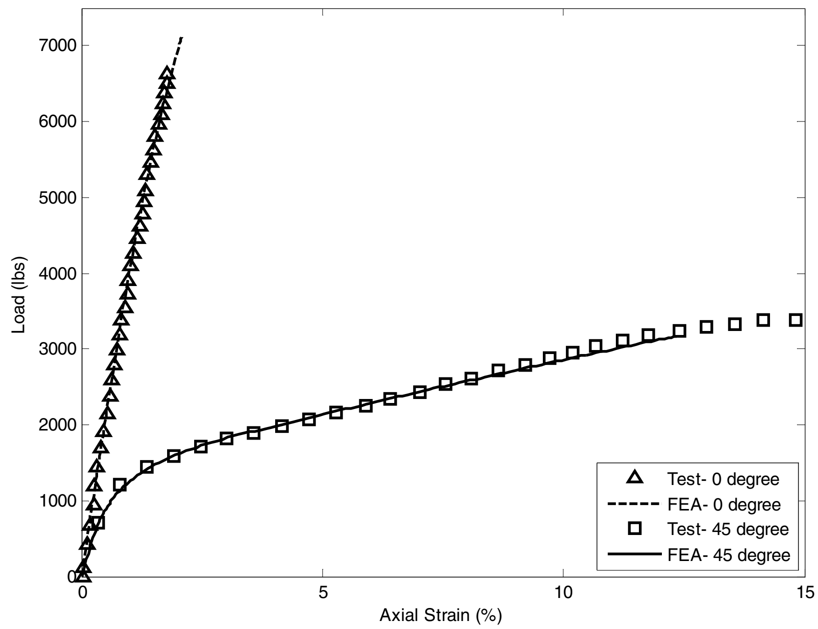

Figure 4. Basic tension, comparison of simulation to digital image test data.

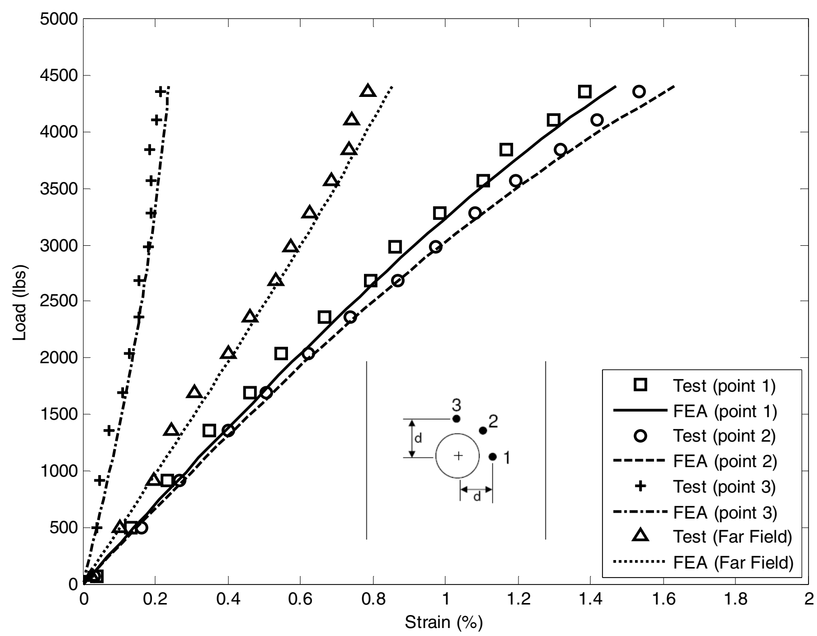

Figure 5. 0 Degree open hole tension, comparison of simulation and test.

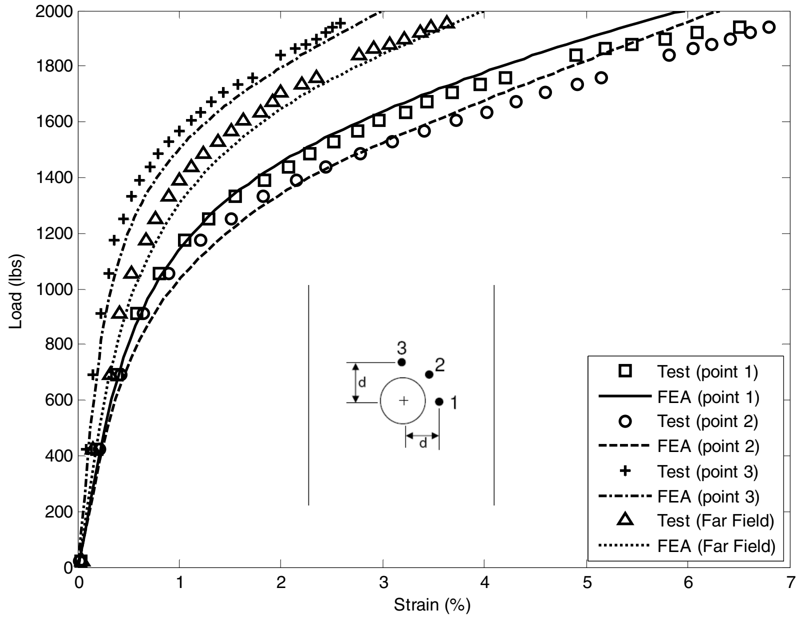

Figure 6. 45 Degree open hole tension, comparison of simulation and test.

Comparisons of strain contours are shown in Figure 7 and Figure 8 for the 0° and 45° open hole tension specimens. The strain contours predicted by the simulation are also in good agreement with digital imaged contours.

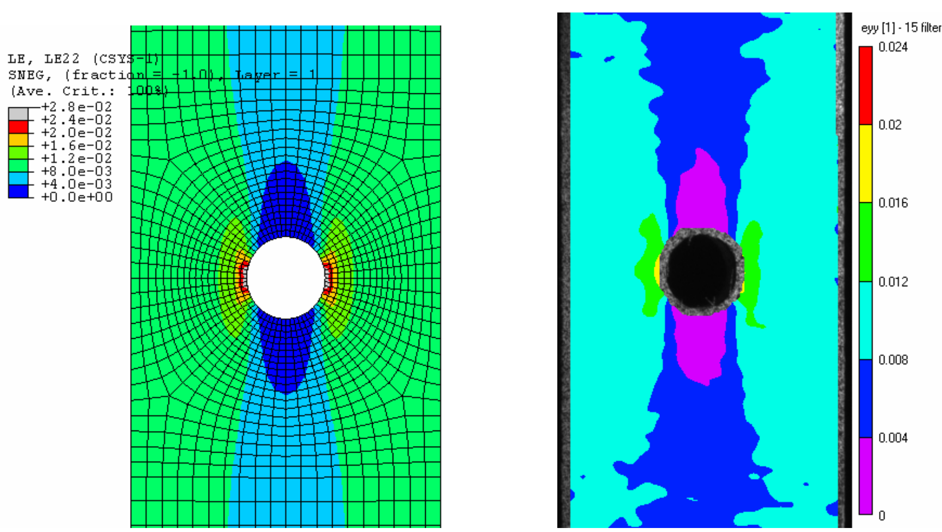

Figure 7. 0° open hole tension, strain contours from simulation and test, 3500 lbs.

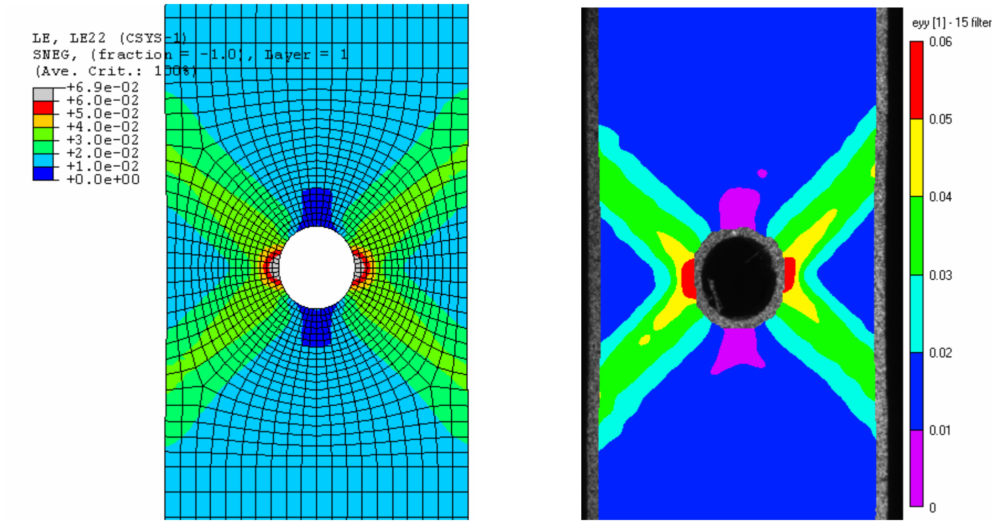

Figure 8. 45° open hole tension, strain contours from simulation and test, 1500 lbs.

Table 2 shows a comparison of the failure loads predicted by the simulation and the peak loads measured by the load cell. The failure loads in the simulation are estimated based on the point where the automatic time incrementation suddenly reduces the step size to a small fraction of the average step size. This reduction would correspond to the rapid change in stiffness that would occur just prior to failure. In general, failure loads predicted by the simulation are within 10% of the actual load, which is *highly significant* and demonstrates the progressive failure methodology is reasonable to characterize the behavior of a woven composite under dynamic loading.

Table 2. Failure load comparison.

Test	Tested Strain Rate (1/s)	Peak Measured Load (lbs)	Simulation (lbs)	% Difference
0° Basic Tension	2.07e-4	6622	7135	7.7
45° Basic Tension	5.44e-4	3421	3172	-7.3
0° Open-Hole Tension	2.85e-4	4447	4403	-1.0
45° Open-Hole Tension	2.88e-4	1970	2088	6.0
0° Open-Hole Tension	0.01	4624	4436	-4.1
0° Open-Hole Tension	0.1	4950	5136	3.8

5. Conclusions

A progressive failure methodology is developed for characterization of woven polymer-based composites under dynamic loading. The approach is implemented in Abaqus via the user defined material subroutine (UMAT). The elements of the progressive failure approach, namely the constitutive theory and the failure theory, are experimentally verified and validated using digital image correlation. This is a relatively new non-contact measurement technique that has proven extremely useful in development of constitutive theory.

Thus far, comparisons of simulation results to test have been encouraging. The progressive failure approach is suitable for characterization of a woven composite subjected to dynamic loads. The constitutive theory and failure theory can account for strain rate dependence, and model parameters are easily adjusted to address other woven composite material systems, other weave patterns, or to perform sensitivity studies.

6. References

1. Soden, P. D., Kaddour, A. S., and Hinton. M. J., "Recommendations for designers and researchers resulting from the world-wide failure exercise", *Composites Science and Technology*, Volume 64, Issues 3-4, March 2004, Pages 589-604
2. Sun, C.T. and Chen, J.L., "A Simple Flow Rule for Characterizing Nonlinear Behavior of Fiber Composites", *J. Composite Materials*, Vol. 23: 1009-1020, 1989
3. Ogihara, S., and Reifsnider, K.L., "Characterization of Nonlinear Behavior in Woven Composite Laminates", *Applied Composite Materials*, Vol 9: 249–263, 2002
4. Weeks, C.A., and Sun, C.T., "Modeling Non-linear Rate-Dependent Behavior in Fiber-Reinforced Composites", *Composites Science and Technology*, Vol. 58: 603-611, 1998
5. Thiruppukuzhi, S.V., and Sun, C.T., "Models for the Strain-Rate-Dependent Behavior of Polymer Composites", *Composites Science and Technology*, Vol. 61: 1-12, 2001
6. Reifsnider, K.L., and Case, S. W., Damage Tolerance and Durability of Material Systems, John Wiley and Sons, 2002
7. Reifsnider, K.L., and Xing, L., "Large-Deformation Constitutive Theories for Structural Composites: Rate-Dependent Concepts and Effect of Microstructure", *strain; An International Journal for Experimental Mechanics,* 2007
8. Xing, L., "Progressive Failure of Large Deformation Woven Composites Under Dynamic Tensile Loading", Ph.D. Dissertation, University of Connecticut, 2007

7. Acknowledgements

The authors would like to thank Dr. Liqun Xing, and Dr. Ken Reifsnider for their help in developing the constitutive theory and determining constitutive model parameters. In addition, the authors gratefully acknowledge the support of Dr. Jeff Hall, Dr. Gale Mulligan, and Mr. Austin Alvarez from General Dynamics - Electric Boat in Groton, CT.

This project was sponsored by the Department of the Navy, Office of Naval Research. Any opinions, findings, and conclusions or recommendations expressed in this material are those of the authors and do not necessarily reflect the views of the Office of Naval Research.